

First-principles calculations of lithium ordering and phase stability on Li_xNiO_2

M. E. Arroyo y de Dompablo, A. Van der Ven, and G. Ceder

Department of Material Science and Engineering, Massachusetts Institute of Technology, Cambridge, Massachusetts 02139

(Received 4 March 2002; published 30 August 2002)

The phase diagram of Li_xNiO_2 ($0 < x < 1$) is calculated using a combination of first-principles energy methods and Monte Carlo simulations. The energy dependence of the Li-vacancy configurational disorder is parametrized with a cluster expansion. At room temperature ordered Li_xNiO_2 phases appear in the phase diagram at $x = 1/4, 1/3, 2/5, 1/2,$ and $3/4$. The predicted lithium-vacancy ordering at $x = 1/4$ and $1/3$ are in good agreement with experiments, while for the other phases no detailed experimental evidence has been reported. We predict a previously undetected phase at $x = 2/5$ to dominate the phase diagram at low lithium content. The stability of ordered Li_xNiO_2 structures is determined by short-ranged repulsive in-plane Li-Li interactions and long-range attractive interplane Li-Li interactions. These attractive interplane Li-Li interactions are due to the Jahn-Teller activity of Ni^{+3} ions. As a result, Li_xNiO_2 behaves fundamentally different from Li_xCoO_2 even though their host structures are identical and Co and Ni have similar ionic sizes.

DOI: 10.1103/PhysRevB.66.064112

PACS number(s): 61.50.Ah

I. INTRODUCTION

Layered LiMO_2 compounds are considered as ideal electrode materials in lithium batteries, due to their high energy density. Among these compounds LiCoO_2 and $\text{LiCo}_{1-x}\text{Ni}_x\text{O}_2$ are currently used in commercial lithium batteries.¹ However the use of LiNiO_2 has been claimed to have cost and toxicity advantages.² Because of the potential application of LiNiO_2 , a considerable interest has been devoted to understanding its electrochemical properties and the phase transformations that occur as a function of lithium content.

LiCoO_2 has been studied thoroughly with experiments^{3,4} as well as first-principles computations.⁵ For this system, theory and experiment are in remarkable agreement, and the computational investigation even predicted a phase at low lithium compositions.⁵ In this paper we present first-principles calculation on Li_xNiO_2 and compare the results to experimental information. These results will demonstrate that the peculiar electronic structure of Ni^{+3} makes LiNiO_2 behave fundamentally different from isostructural LiCoO_2 , even though Co and Ni have similar ionic sizes.

LiNiO_2 is isostructural with $\alpha\text{-NaFeO}_2$, having an ordered rock salt structure in which alternate layers of Li^+ and Ni^{+3} ions occupy octahedral sites within the fcc oxide array⁷ (see Fig. 1). Trivalent nickel with an electronic configuration $(t_{2g})^6(e_g)^1$ is a potential Jahn-Teller active ion. However, LiNiO_2 adopts rhombohedral symmetry in the space group $R\bar{3}m$ at any temperature,⁸ with Li in $3a$, Ni in $3b$ and O in $6c$ sites. During the cycling of a lithium cell the lithium ions are reversibly removed from and reinserted into this structure creating or annihilating vacancies within the lithium planes. These vacancies can organize to form ordered lithium-vacancy structures on a triangular lattice of sites, or they can indirectly drive electronic transitions as in the case of LiCoO_2 .^{5,6} The sequence of phase transitions that occurs during the lithium intercalation and deintercalation in Li_xNiO_2 is still unclear. Initial studies indicated that lithium could be deintercalated from LiNiO_2 without changing the rhombohe-

dral symmetry.⁹⁻¹² This single-phase picture has been supplanted, and lithium extraction from LiNiO_2 is believed to take place through four single-phase regions: rhombohedral 1, monoclinic, rhombohedral 2, and rhombohedral 3,¹³⁻¹⁷ though some discrepancies still exist.¹⁸ Figure 2 shows some of the different phase diagrams that have been proposed based on electrochemical data and x-ray diffraction studies.^{2,14,15,17} In the range $0.75 < x < 1$ the rhombohedral symmetry of the starting compound is maintained. Between

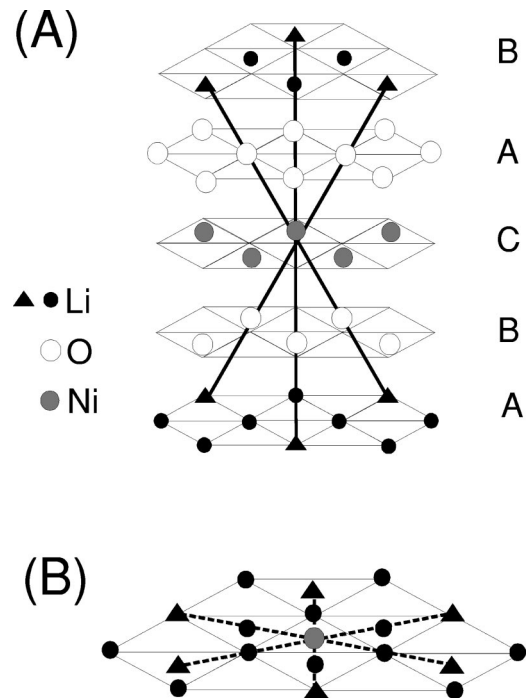


FIG. 1. (a) Schematic representation of the LiNiO_2 structure. The oxygen ions form a close-packed array, with Ni^{+3} and Li^+ ions alternating in the (111) planes. The triangles indicate Li ions which are at the extension of the Ni-O bond from the central Ni ion. Filled circles indicate other lithium ions. (b) Projection of the structure onto the basal plane showing two planes of lithium ions, A and B, and the interplane $\text{Li}_A\text{-Li}_B$ interactions through the central Ni ion as dashed lines.

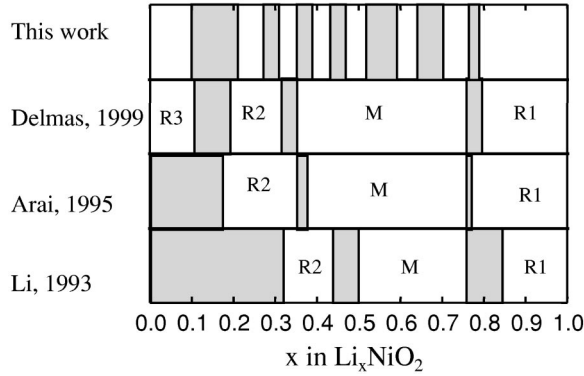


FIG. 2. Phase diagrams proposed from experimental studies, taken from Refs. 14, 15, and 17. The results from this work are also shown for comparison. White and gray areas, respectively, denote single- and two-phase regions.

$\text{Li}_{0.5}\text{NiO}_2$ and $\text{Li}_{0.75}\text{NiO}_2$ a monoclinic region has been found, although some controversy exists regarding the actual nature and stability range of this monoclinic phase. For compositions below $\text{Li}_{0.3}\text{NiO}_2$ a rhombohedral symmetry is stable, but with a drastic change of cell parameters that limits the reversible intercalation domain to the range $0.3 < x < 1$.^{13,19} As observed in Fig. 2, three two-phase regions have been detected, indicating that transformations take place through first-order transitions. Ordered structures have been proposed at $\text{Li}_{0.25}\text{NiO}_2$,^{15,17} $\text{Li}_{0.33}\text{NiO}_2$,¹⁷ $\text{Li}_{0.5}\text{NiO}_2$,^{15,17,19,20} $\text{Li}_{0.63}\text{NiO}_2$,^{17,20} and $\text{Li}_{0.75}\text{NiO}_2$,^{15,17,20} though experimental evidence has been reported only at $x = 1/4$, $1/3$, and $\text{Li}_{0.63}\text{NiO}_2$.^{17,20}

A clear understanding of this compound is complicated by the excess Ni that is always present in the prepared materials. Hence the compound is more accurately denoted by $\text{Li}_{1-z}\text{Ni}_{1+z}\text{O}_2$.^{2,7} The excess nickel replaces Li ions in the 3a sites and has valence 2+. The real formula of the compound should therefore be expressed as $[\text{Li}_{1-z}\text{Ni}_z^{+2}]_{3a}[\text{Ni}_{1+z}\text{Ni}_z^{+2}]_{3b}[\text{O}_2]_{6c}$.²¹ Several investigations have indicated that Ni^{2+} ions in the 3a sites strongly affect the voltage profile and reversibility of the intercalation reaction.^{2,15-17,22-24}

As first-principles calculations yield detailed information about relative stability and local structure as a function of composition, they may be useful to further clarify the phase diagram of Li_xNiO_2 . First principles refers to the use of quantum mechanics to determine the structure and electronic properties of materials. In recent years first-principles methods have been successfully used to study cathode materials for rechargeable lithium batteries.^{5,6,25-29} Through a combination of first-principles total-energy calculations and statistical mechanics we obtain the phase stability of Li_xNiO_2 as a function of concentration and temperature. In Secs. III A and III B we calculate the total energy of a set of Li_xNiO_2 structures at 0 K to determine the ground states and the relative energy differences between structures. In Sec. III C the ground states are discussed and some rationalization of their stability is attempted. In Sec. III D we construct and calculate a free-energy model to determine the phase stability at non-zero temperature. This free-energy model also enables us to

predict the voltage profile of a Li/LiNiO_2 cell, which is compared to the experimental voltage-composition curve in Sec. III E.

II. METHOD

The theoretical background to obtain a phase diagram from first-principles calculations can be found in some of our previous work,^{5,6} so it is only briefly summarized in this paper. The methodology followed in this work is similar to that used for Li_xCoO_2 ,⁵ although the local Jahn-Teller (JT) distortion in Li_xNiO_2 adds some subtle complexities. The formalism consists of three parts.

(i) First-principles total-energy calculations of different ordered arrangements of lithium ions and vacancies within the NiO_2 host are performed.

(ii) These energies are then used to parametrize a cluster expansion that describes the energy of Li_xNiO_2 in terms of an Ising-like Hamiltonian. A well-converged cluster expansion enables an accurate and rapid extrapolation of the total energy of any lithium-vacancy configuration from the first-principles energy values calculated in the first step.

(iii) The cluster expansion is then used in Monte Carlo simulations to calculate thermodynamic properties and equilibrium phase boundaries.

To calculate the total energy of ordered Li_xNiO_2 structures we use the *ab initio* pseudopotential method as implemented in the Vienna *ab initio* simulation package (VASP).^{30,31} This method solves the Kohn-Sham equations within the local-density approximation (LDA) or the generalized gradient approximation (GGA) using ultrasoft pseudopotentials. In previous work^{32,33} we found the use of GGA, rather than LDA, to be essential for correctly reproducing the Jahn-Teller distortion in Mn^{+3} compounds. Since Ni^{+3} is potentially Jahn-Teller active, all calculations in this work were performed within the generalized gradient approximation. A plane-wave basis set with a kinetic-energy cutoff of 400 eV was used. The reciprocal space sampling was done with a $6 \times 6 \times 6$ k -point grid for structures containing 2 LiNiO_2 f.u., and a $4 \times 4 \times 4$ or $2 \times 2 \times 2$ k -point grid for larger supercells so as to approximately keep the absolute k -point density constant. Relaxation was allowed and the final energies of the optimized geometries were recalculated so as to correct for changes in the plane-wave basis during relaxation.

To obtain a good cluster expansion it is critical that one finds the lowest energy for a given Li-vacancy ordering. In most systems it suffices to relax the structure consistent with the symmetry imposed by the Li-vacancy ordering in the host. If spontaneous symmetry breaking that is not due to Li-vacancy ordering can occur, such symmetry reduction needs to be explicitly allowed for. In Li_xNiO_2 the symmetry can be reduced by collective JT distortions that are independent of the symmetry reduction by Li-vacancy ordering. To investigate this effect we will report on two sets of results, one where the symmetry of the initial host is taken as rhombohedral and which may or may not allow for JT distortions depending on the symmetry of the Li-vacancy ordering, and another one where the symmetry of the initial host is taken as

monoclinic so that JT distortions are always possible. A cluster expansion was fitted to the calculated energies. Statistical significance of this fit was ensured with the cross-validation technique. A detailed description of this method is reported in Ref. 34. The cluster expansion was then implemented in Monte Carlo simulations in the grand canonical ensemble. To study the thermodynamics of Li and vacancy ordering in Li_xNiO_2 , we used a Monte Carlo cell containing 5400 LiNiO_2 unit cells. At each temperature and chemical potential, at least 2000 Monte Carlo passes per lattice sites were performed after which sampling occurred over a minimum of 4000 Monte Carlo passes.

III. RESULTS

A. Host structures and symmetry

LiNiO_2 , as LiCoO_2 , crystallizes in a layered host structure where the oxygen slabs have an $ABCABC$ stacking sequence. This host is denoted by O3. The layered structure of LiCoO_2 is retained upon lithium deintercalation, but in Li_xCoO_2 at low lithium concentrations, different oxygen stackings of the type $ABAB$ ($x=0$) and $ABABCACABCBC$ ($0 < x < 0.3$) are found.^{35,36} These hosts have been denoted as O1 and H1-3, respectively, H1-3 being a hybrid of the O1 and O3 phase. Fully delithiated CoO_2 is stable in the O1 host, where the Li-O octahedra share faces with the Co-O octahedra, whereas in the O3 host they share edges. As Li fills the sites of CoO_2 , the O3 host becomes more stable than the O1 host, since the former phase minimizes the repulsion between the Li and the Co ions. In the $\text{Li}_{1-z-x}\text{Ni}_{1+z}\text{O}_2$ system, a recent x-ray-diffraction study of highly delithiated samples has also shown the formation of the O1 host structure near the NiO_2 composition.³⁷ This only happens when the amount of extra Ni ions in the interslab space is small, $z < 0.07$. We have calculated the relative stability of NiO_2 within the O1 and O3 hosts and found the O1 host structure to be 7 meV f.u. below that of the O3 host structure. However, this energy difference between the O1 and O3 hosts is small in comparison with the 40 meV/f.u. calculated for CoO_2 .⁵ The different relative stabilities of the O1 and O3 hosts in the two systems is likely connected to the electronic nature of the transition metal. Co^{+4} has a $(t_{2g})^5$ configuration and Ni^{+4} a $(t_{2g})^6$ configuration. Complete filling of the t_{2g} orbitals in NiO_2 may make it less conducive to covalent bond formation with oxygen and therefore reduce the relative stability of the O1 stacking sequence with respect to that of the O3 host. In the present work we have limited the study of Li_xNiO_2 to the O3 host structure. Because of the potential Jahn-Teller activity of Ni^{+3} ions, the symmetry of Li_xNiO_2 can be reduced by a collective Jahn-Teller distortion, independently of the symmetry reduction by Li-vacancy ordering. Therefore we have considered results from two different sets of energy calculations.

(i) Energies of ordered structures whereby the symmetry of the host is taken as rhombohedral. Hence the symmetry of the ordered Li-vacancy superstructure is necessarily a subgroup of the $R\bar{3}m$ group. Depending on the particular Li-vacancy ordering, this subgroup symmetry may or may not allow Jahn-Teller distortions.

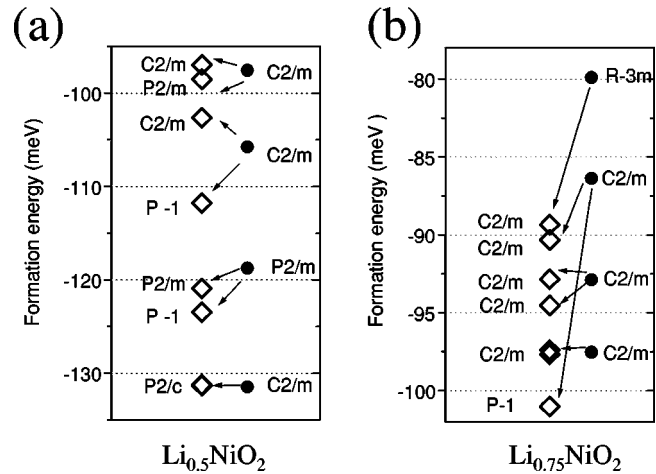


FIG. 3. Calculated formation energy of Li_xNiO_2 at (a) $x=0.5$ and (b) $x=0.75$. Filled circles denote structures calculated in subgroups of the rhombohedral LiNiO_2 symmetry, and open diamonds indicate structures in subgroups of the monoclinic host. Ordered structures with the same lithium-vacancy arrangement but different host symmetry are connected by arrows. The space group of the final relaxed structure is also given.

(ii) Energies of ordered structures whereby the symmetry of the host is taken as monoclinic $C2/m$. Since in this case the symmetry of the ordered Li-vacancy superstructure is a subgroup of $C2/m$, a collective Jahn-Teller distortion is always possible. Due to the monoclinic symmetry breaking in $C2/m$, most Li-vacancy ordering in the rhombohedral host have two distinct Li-vacancy orderings in the monoclinic host. The two ordered states differ by their orientation with respect to the monoclinic axis.

Since all the possibilities of (i) are included in (ii), starting from the monoclinic host, in principle, always give the lowest energy. The latter energy may be equal to the energy-derived form of the rhombohedral host if no JT distortion occurs. We found that at low lithium concentrations ($x < 0.4$) there was no energy difference between ordered configurations relaxed from the monoclinic or rhombohedral host, consistent with the idea that the low number of Ni^{+3} ions cannot create a collective JT distortion unless the symmetry is already broken by the Li-vacancy ordering. However at higher lithium concentrations the situation is more complex. Figure 3 shows the formation energy of several Li_xNiO_2 ordered structures with $x=0.5$ [Fig. 3(a)] and $x=0.75$ [Fig. 3(b)]. Filled black circles and open diamonds indicate Li configurations obtained from r - LiNiO_2 and m - LiNiO_2 , respectively. Arrows connect structures with the same Li-vacancy ordering but different host symmetry. As illustrated in Fig. 3, any of the r - Li_xNiO_2 ordered structures splits into two different structures when the symmetry of the host is $C2/m$. For the same Li-vacancy ordering the energy is lower within the monoclinic host (open diamonds) than within the rhombohedral host (filled circles). For instance, the energy of the most stable $\text{Li}_{0.75}\text{NiO}_2$ structure within the rhombohedral host is lowered by 15 meV in the monoclinic host. In Fig. 3 it can also be seen that m - Li_xNiO_2 structures with the same Li-vacancy ordering, but oriented differently

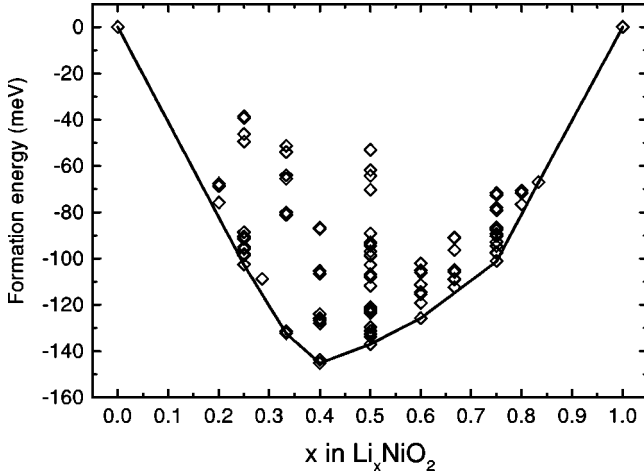


FIG. 4. Calculated formation energies of ordered Li_xNiO_2 structures as a function of the lithium concentration.

along the monoclinic axis, have energies as different as 10 meV. The final symmetry of the relaxed structures is also indicated in Fig. 3. Notice that the symmetry of $r\text{-Li}_x\text{NiO}_2$ structures is in most cases monoclinic, whereas the Li_xNiO_2 structures in the monoclinic host can lower their symmetry to triclinic.

From this section we conclude that the lowest energy for a given Li-vacancy ordering is acquired by relaxing from a monoclinic host, where the symmetry can be reduced by collective JT distortions, and not merely by the Li-vacancy ordering.

B. Formation energies and cluster expansion

The total energy of 100 Li_xNiO_2 structures was calculated at values of $x = 1/5, 1/4, 2/7, 1/3, 2/5, 1/2, 3/5, 2/3, 3/4, 4/5$, and $5/6$. Many different lithium-vacancy arrangements were considered at most lithium concentrations. The structures that are actually stable at low temperature out of this large set can be found by constructing the convex hull of the formation energies. We define the formation energy for a given Li-vacancy distribution with composition x as

$$\Delta_f E = E - xE_{\text{LiNiO}_2} - (1-x)E_{\text{NiO}_2}, \quad (1)$$

where E is the total energy of the configuration per $\text{Li}_x\text{Ni}_{1-x}\text{O}_2$ formula unit, E_{LiNiO_2} is the energy of LiNiO_2 in the monoclinic host, and E_{NiO_2} is the energy of NiO_2 in the monoclinic host.

The formation energies of the Li_xNiO_2 structures are plotted in Fig. 4. The numerical error in the energy is about 5 meV, as estimated by performing convergence tests of the calculated total energy E with respect to the k -space grid and the basis set cutoff energy, and it is unrelated to any physical errors that may occur from the GGA approximation in the density functional theory. It can be observed in Fig. 4 that all the Li_xNiO_2 structures considered have negative formation energy, indicating that they are stable with respect to phase separation into LiNiO_2 and NiO_2 . This is a sign of repulsive Li-Li interactions and indicates that Li-vacancy ordering will

occur. In Fig. 4 it can also be seen that at a given lithium concentration the formation energy of different Li_xNiO_2 structures is quite similar in many cases. This indicates that the Li ions do not interact strongly but are screened by the local oxygen environment. This characteristic was also noticed in the study of Li_xCoO_2 .⁵ Charge transfer and screening in layered LiMO_2 compounds have been treated in detail in Refs. 5, 38 and 39.

The formation energies of Li_xNiO_2 allow us to determine the ground-state energy vs composition curve (convex hull), which is drawn in Fig. 4. The convex hull is the set of tie lines that connects all the lowest-energy ordered phases. When the energy of a particular ordered structure is above a tie line, it is unstable with respect to a mixture of the two structures that define the end points of the tie line. The convex hull can be viewed as the free energy at 0 K where entropy is absent. It, therefore, determines phase stability at zero temperature. This curve has several vertices at which characteristic ordered structures of lithium ions and vacancies appear. In Li_xNiO_2 , ground states occur at $x = 1/4, 1/3, 2/5, 1/2, 3/5, 3/4$, and $5/6$.

To study the Li-vacancy ordering at nonzero temperature one has to account for entropy, the most important of which is configurational entropy due to Li-vacancy substitutional exchanges. Thermal equilibration of the Li-vacancy arrangement can be achieved by Monte Carlo simulations on an appropriate lattice model Hamiltonian^{40,41} through a procedure that is well established.⁴² The lithium-vacancy arrangement in a particular structure is represented by occupation variables σ_i , which are defined on the lattice at all possible sites where Li ions can sit ($\sigma_i = +1/-1$ when the site is occupied/vacant). The energy of Li_xNiO_2 is then expanded in polynomials ϕ_α of these occupation variables σ_i :

$$E = V_0 + \sum_{\alpha} V_{\alpha} \phi_{\alpha}. \quad (2)$$

Equation (2) is usually referred to as a cluster expansion.^{41,42} The function ϕ_{α} is defined as a product of occupation variables $\sigma_i \sigma_j \sigma_k$, where the indices i, j, k correspond to a collection of sites that form a cluster α , such as a pair cluster, triplet cluster, etc. V_0 and V_{α} are called the effective clusters interactions (ECI) and are constant. The ECI are merely expansion coefficients describing the dependence of the energy of the crystal on the Li-vacancy configurations and are determined by fitting the calculated energy of the ordered structures to Eq. (2). A subset of the 100 calculated energies in the monoclinic host were used to determine the ECI of Eq. (2). Our experience indicates that in this system better cluster expansions are obtained by using small and simple clusters and structures. For this reason only structures with up to four LiNiO_2 unit cells were used in the fit. A cluster expansion with rhombohedral symmetry was used. As noted earlier, most ordered lithium-vacancy arrangements within the rhombohedral NiO_2 host have two crystallographically distinct variants within the monoclinic host. Of each of the two distinct variants within the monoclinic host, we used that with the lowest energy in the fit of the ECI. This reduces the number of structures considered in the fit from 100 to 37,

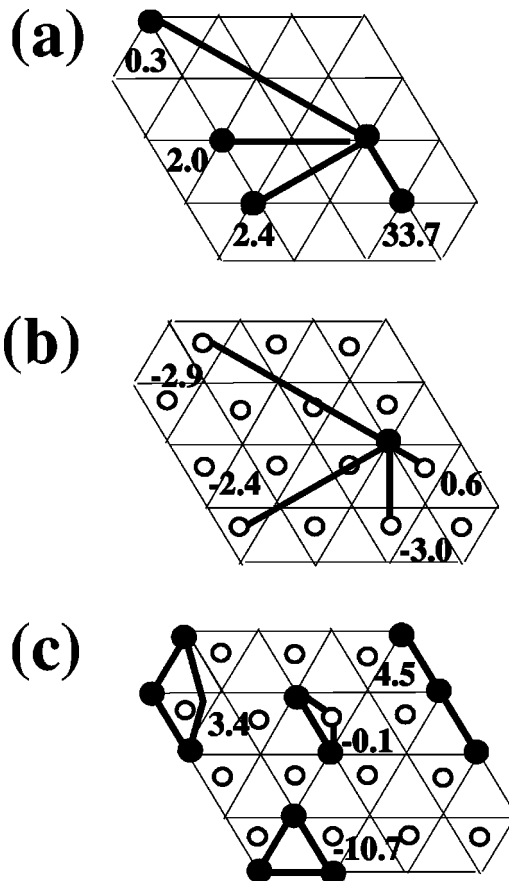


FIG. 5. In-plane pairs (a), interplane pairs (b), and triplets (c) used in the cluster expansion. The triangular lattice denotes the Li sites within a single plane, while the unfilled circles denote the projection of an adjacent Li plane. The value of the interactions is given in meV. Negative three-body interactions indicate an effective interaction that is attractive between Li ions.

and the cluster expansion was finally performed over 31 different lithium-vacancy configurations. The resulting cluster expansion contains eight pairs and four triplets. The root-mean-square (rms) difference between the 31 formation energy values used in the cluster expansion and the corresponding values as calculated with the pseudopotential method and as predicted by the cluster expansion is ≈ 6 meV. For the remaining six Li-vacancy configurations not included in the inversion, the rms difference between their energies as calculated with the pseudopotential method and as predicted by the cluster expansion is 8 meV. When considering those critical structures containing more than four unit cells, as some of the detected ground states, the rms difference is still below 10 meV, consistent with a calculated cross validation score of 9 meV. Cross-validation scores are a measure of the accuracy of the cluster expansion in predicting the energy of structures not used in the fit.³⁴

Figure 5 shows the ECI used in the cluster expansion as well as their value. The upper panel corresponds to in-plane lithium interactions, the middle panel shows interactions between two consecutive planes of lithium ions, and the bottom panel shows the three-body interactions. Positive interactions indicate Li-Li repulsion, whereas negative values indicate an effective attraction. The in-plane interactions [Fig. 5(a)] are

repulsive and decaying with distance. The significant decrease in going from the first neighbors to the next neighbors indicates again a very strong screening in these structures.

In Li_xNiO_2 structures, different Li planes are far apart as they are separated by O-Ni-O slabs. The ECI corresponding to clusters connecting different lithium planes are therefore expected to be weak. Indeed this is observed in Fig. 5(b) for the interaction between a lithium ion and its closest neighbor in the next plane. Since interactions between lithium ions in one plane and the first neighbor in the next plane are weak, it is expected that interactions with further neighbors would be even weaker, as found in Li_xCoO_2 .⁵ Contrary to this, in Li_xNiO_2 non-negligible attractive interactions exist between Li ions in different planes. In previous work³³ we explained this interaction through the coupling of the Li ions with the JT distortion of Ni^{3+} centers. In particular, the interaction with value -2.4 meV in Fig. 5(b) is between Li ions that are on the extensions of linear O-Ni-O bonds. A better description of this interplane Li-Li interaction can be seen in Fig. 1, where the Li ions interacting in different planes (A and B) are denoted by triangles. These lithium ions form $180^\circ \text{Li}_A\text{-O-Ni-O-Li}_B$ configurations, which have been treated in detail in Ref. 33. This Li-Li interaction is attractive as the presence of Li ions on both ends of this O-Ni-O segment significantly lowers the presence of the filled $\text{Ni}^{3+} e_g$ orbital and enhances the JT activity. These interplane interactions turn out to be crucial for stabilizing some of the ordered ground states in the phase diagram.

C. Ground states in Li_xNiO_2

Figure 6 shows the ground-state Li-vacancy arrangements. Two successive planes of lithium ions are shown, with large and small filled black circles, respectively. For these structures, the approximate charge around each Ni ion has been calculated by integrating the unpaired electron density within a sphere of a radius 1.5 \AA centered at the different Ni sites.³³ These charges have been rounded off to $+3$, $+4$, and $+3.5$, depending on which of the three formal valence states is closest to the integration result. In Fig. 6, Ni^{+3} ions are indicated by dark gray circles, $\text{Ni}^{+3.5}$ ions by light gray circles, and Ni^{+4} ions by white circles. For clarity only the Ni ions in one unit cell are shown.

The in-plane ordering of the ground states at $x = 1/4$, $1/3$, and $3/4$ is rather common on a triangular lattice.^{6,43,44} These types of arrangements are expected when Li-Li repulsive interactions dominate⁶ and indeed these structures were also found as lowest-energy configurations in Li_xCoO_2 in the O3 host, although only $\text{Li}_{0.33}\text{CoO}_2$ was stable up to room temperature.⁵ At $x = 1/2$ the most frequent ordering consists of alternate rows of lithium and vacancies,^{6,44} a structure found from experiments and calculations in $\text{Li}_{0.5}\text{CoO}_2$.^{3,5} However, $\text{Li}_{0.5}\text{NiO}_2$ has a different ground state, 13 meV more stable than the ordering exhibited by $\text{Li}_{0.5}\text{CoO}_2$. The Li-vacancy distribution in $\text{Li}_{0.4}\text{NiO}_2$ agrees with that described by Kaburagi and Kanamori an enumeration of possible ground-state ordering on the triangular lattice at that composition.⁴⁴ Remarkably, this ordered phase has not been considered in any of the previous work on the LiNiO_2 sys-

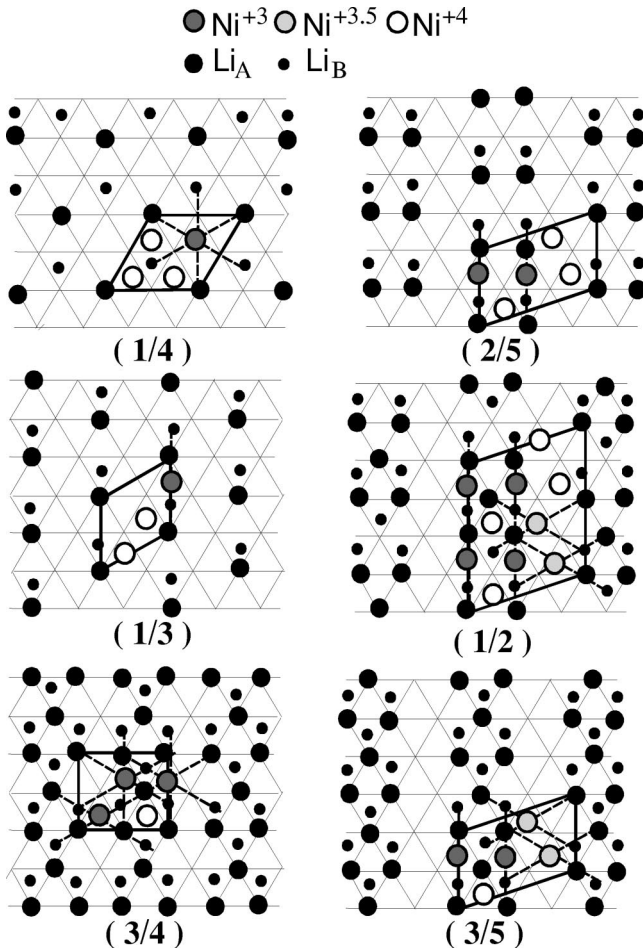


FIG. 6. Lowest-energy lithium-vacancy arrangements in Li_xNiO_2 at x values of $1/4$, $1/3$, $2/5$, $1/2$, $3/5$, and $3/4$. The big black circles denote the in-plane lithium orderings and the small black circles designate the positions of the Li ions in the adjacent plane. Dashed line indicates the 180° Li-O-Ni³⁺-O-Li configurations. Ni³⁺ ions are indicated by dark gray circles, Ni^{3.5+} ions by light gray circles, and Ni⁴⁺ ions by white circles.

tem. To our knowledge the ordered superstructures we found as ground states at $\text{Li}_{0.5}\text{NiO}_2$ and $\text{Li}_{0.6}\text{NiO}_2$ have never been reported before in any other physical or theoretical system. Notice that the supercells in these peculiar cases are related. In $\text{Li}_{0.4}\text{NiO}_2$, nearest-neighbor lithium dimers line up to form “dimer rows.” By half filling the sites in between the two parallel rows $\text{Li}_{0.5}\text{NiO}_2$ is obtained, whereas $\text{Li}_{0.6}\text{NiO}_2$ corresponds to the complete filling of the sites in between two parallel rows. The double rowed dimers seem to be the stable unit of these structures as is also evident from the large stability of the $\text{Li}_{0.4}\text{NiO}_2$ structure.

For a given in-plane lithium-vacancy ordering, adjacent Li planes can stack in different ways. In systems where interplane Li-Li interactions are weak the energy difference between distinct stacking sequences is small. But in the case of Li_xNiO_2 , where strong Jahn-Teller induced interplanar interactions have been documented,³³ particular stacking sequences may be favored. Figure 6 shows for each structure the most stable stacking. As in Ref. 33, we find that at each composition the lowest-energy structure has Li-Li or □-□

pairs along the O-Ni³⁺-O extensions, but never a Li-□ pair. These $\text{Li}_A\text{-O-Ni}^{3+}\text{-O-Li}_B$ complexes are shown by the dotted lines in Fig. 6. This is consistent with the attractive interactions observed in the cluster expansion along this direction. The result of the charge integrations around Ni ions, shown in Fig. 6, indicates clearly that distinct valence states of the Ni ions exist in partially delithiated materials. This is unlike Li_xCoO_2 where the effective charge on the transition metal is delocalized over all Co ions and the material is metallic when enough Li is removed.^{5,33} In the low-energy configurations the unit cell for Ni-charge ordering is always equivalent to the lithium-vacancy ordering, another indication that there is a strong codependence between the Li-vacancy configuration and Ni³⁺-Ni⁴⁺ ordering.

It can be seen in Fig. 6 that for $x > 0.4$, Ni⁴⁺ ions occupy sites fully coordinated by lithium ions. This is a very symmetrical environment favorable for a nonactive JT ion, such as Ni⁴⁺. The effect of this can be seen in the nearest-neighbor triplet interaction [-10.7 meV in Fig. 5(c)] which is strongly attractive, weakening the effect of the nearest-neighbor repulsion. Based on electrostatic considerations one would expect the nearest neighbors of Ni⁴⁺ to be Li vacancies. However, as was explained in Ref. 33, the occupied e_g orbital in Ni³⁺ favors a Li ion in the second neighbor position, along the extension of the $e_g(\text{Ni})\text{-}p(\text{O})$ orbital. This tends to force Li ions into a nearest-neighbor position to Ni⁴⁺. The interactions on Fig. 5 are a good example to demonstrate that many physical effects, other than electrostatics, contribute to the effective Li-Li interactions. While in Li_xCoO_2 the interactions display typical electrostatic behavior,⁵ with strong screening by oxygen, in Li_xNiO_2 the interactions are much more influenced by the charge distribution and electronic structure of Ni.

D. Phase diagram

The phase diagram of Li_xNiO_2 is determined by Monte Carlo simulation on the cluster expansion of Fig. 5. By integrating the chemical potential, the free energy as a function of the lithium concentration can be determined. In this section we present the calculated phase diagram of stoichiometric Li_xNiO_2 . In addition, knowledge of the chemical potential allows a calculated voltage composition to be compared with the experimental curve (Sec. III E).

Figure 7 shows the calculated equilibrium phase diagram for Li_xNiO_2 . The various ordered regions are shown in gray and are separated by domains of two-phase coexistence. Hence, at room temperature all phase transitions detected in this system are first order. The insets of Fig. 7 show the in-plane lithium-vacancy arrangement of the ordered states. The phase diagram is only shown for $T > 250$ K, as equilibrium was difficult to achieve in the Monte Carlo simulations at low temperature. Several interesting observations are to be made about the calculated phase diagram. All ground states from Fig. 4 appear in the phase diagram except for the ordered structures at $x = 0.6$ and $x = 5/6$ which disorder at low temperature. Surprisingly, the structure at $x = 0.4$, with the ordered Li-Li dumbbells dominates the phase diagram at low lithium concentration. The structures at $x = 0.5$ and 0.75 dis-

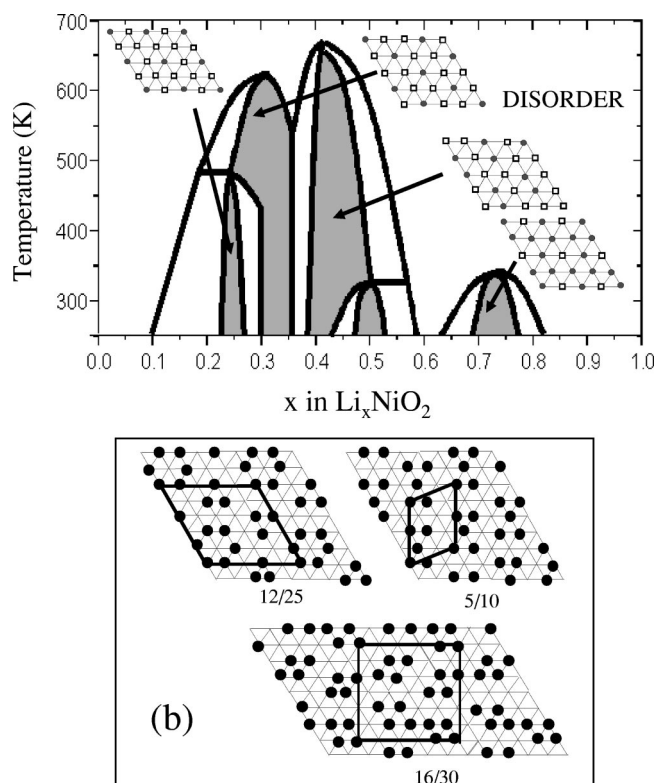


FIG. 7. (a) Calculated phase diagram of Li_xNiO_2 . The gray areas represent ordered Li_xNiO_2 regions. The insets show the Li-vacancy distribution in the ordered structures stable at room temperature. (b) Additional Li_xNiO_2 ordered structures found in Monte Carlo simulation at $x=0.48$ and $x=0.533$, and the ground state at $x=0.5$.

order around room temperature, though one could expect the order-disorder temperature to be overpredicted as in the case of Li_xCoO_2 .⁵ The general increase of the order-disorder temperature towards lower lithium concentration is due to the reduced charge on oxygen as Li is removed, which decreases the screening of the Li^+-Li^+ interaction.

The Monte Carlo simulation has also identified new structures. This is one of the advantages of the cluster expansion approach: once the cluster expansion is well parameterized using the energy of structures with small unit cells, the energy of any arrangement can be rapidly obtained. Hence, completely new structures can be predicted as ground states. Figure 7(b) shows two new Li_xNiO_2 structures identified in the Monte Carlo simulation, with $x=0.48$ and 0.533 , as well as the ground state for $\text{Li}_{0.5}\text{NiO}_2$. Due to the large size of the $\text{Li}_{0.48}\text{NiO}_2$ and $\text{Li}_{0.533}\text{NiO}_2$ unit cells, their energy was not calculated from first principles. In these structures of Fig. 7(b), lithium ions form nearest-neighbor triangles. It is likely that they surround the Ni^{4+} ions in the structure. This area of the phase diagram was not resolved in detail due to the difficulty in obtaining well-equilibrated structures.

Experimentally, ordered Li_xNiO_2 structures have been detected by selected area electron diffraction at $x=1/4$ and $x=1/3$.¹⁷ The lithium-vacancy distributions proposed from experiments in $\text{Li}_{1/4}\text{NiO}_2$ and $\text{Li}_{1/3}\text{NiO}_2$ agree with those shown in Fig. 7. Electrochemical experiments also seem to suggest the presence of ordered $\text{Li}_{1/2}\text{NiO}_2$ and $\text{Li}_{3/4}\text{NiO}_2$ dur-

ing the cycling of Li/LiNiO_2 cells.^{15,19,45,46} However, to our knowledge, the specific nature of the Li ordering has not been investigated at these compositions. Several authors have speculated that in $\text{Li}_{1/2}\text{NiO}_2$, lithium and vacancies should order in alternate rows, as was found in LiCoO_2 .^{15,19,20} It has been assumed that $\text{Li}_{3/4}\text{NiO}_2$ has the same ordered structure as $\text{Li}_{1/4}\text{NiO}_2$ but with lithium and vacancies exchanged.^{15,20,45} Thus in $\text{Li}_{1/2}\text{NiO}_2$ and $\text{Li}_{3/4}\text{NiO}_2$ the calculated most stable Li-vacancy arrangement differs from previously proposed (but not confirmed) models. Nevertheless, the energy difference between the calculated lowest-energy Li-vacancy distributions and those previously proposed.^{15,19,20} is small in $\text{Li}_{3/4}\text{NiO}_2$ (4 meV), and relatively small in $\text{Li}_{1/2}\text{NiO}_2$ (13 meV). These small differences in energy make it difficult to unambiguously decide which ground state is stable. In order to discriminate between the two possibilities more detailed experimental data is required. Evidence of lithium ordering has also been found by selected area electron diffraction (SAED) in $\text{Li}_{0.63}\text{Ni}_{1.02}\text{O}_2$.²⁰ The SAED pattern can be interpreted with a $2 \times 2 \times 2$ superstructure of a monoclinic cell with $a=4.988 \text{ \AA}$, $b=2.828 \text{ \AA}$, $c=5.069 \text{ \AA}$, and $\beta=109.75^\circ$.⁴⁷ In the model proposed by Peres *et al.*²⁰ this superstructure is derived from the hypothetical ordered states at $x=0.5$ and 0.75 by the half-filling of the positions that are empty at $x=0.5$ but filled at 0.75 . Hence the stoichiometry of this compound would be $\text{Li}_{5/8}\text{NiO}_2$. In the calculated phase diagram at that lithium concentration there is no ordered phase. Instead, a two-phase region is present where $\text{Li}_{0.75}\text{NiO}_2$ and a solid solution coexist. Within this picture, any evidence of ordering should come from the $\text{Li}_{0.75}\text{NiO}_2$ superstructure which has parameters $2a_m \times b_m \times c_m$ and $P-1$ symmetry. This symmetry is inconsistent with the experimental electron-diffraction patterns. Hence, for this region of the phase diagram there seems to be clear discrepancy between calculated and experimental results.^{17,20} Calculations predict a strong ordered phase at $x=0.4$ with $C2/m$ symmetry. Interestingly, the existence of an ordered $\text{Li}_{0.4}\text{NiO}_2$ has not been considered in the literature, although the experimental voltage-composition curve [see Fig. 8(a)] exhibits a voltage step around that composition. Powder x-ray-diffraction data taken in $\text{Li}_{0.38}\text{Ni}_{1.02}\text{O}_2$ and $\text{Li}_{0.4}\text{Ni}_{1.008}\text{O}_2$ reveal that this composition corresponds to a single phase of monoclinic symmetry.^{48,49} Further experimental characterization in this area of the phase diagram is therefore desirable.

The calculated phase diagram corresponds to stoichiometric LiNiO_2 . However, in LiNiO_2 some departure from stoichiometry is unavoidable, and a compound $\text{Li}_{1-z}\text{Ni}_{1+z}\text{O}_2$ is obtained.^{17,21,23} The excess Ni ions are present in the interslab space in the form of Ni^{2+} ions occupying lithium positions. To charge compensate these ions, $z\text{Ni}^{2+}$ ions must also be present in the NiO_2 layer. For small values of z the introduction of some disorder in LiNiO_2 will decrease the temperature of the order-disorder transitions. Hence, depending on the degree of disorder, at room temperature not all the ground states predicted for LiNiO_2 may be detected in off-stoichiometric $\text{Li}_{1-z}\text{Ni}_{1+z}\text{O}_2$. At large enough values of z , the Ni^{2+} ions statistically distributed within the lithium sites could completely prevent any Li-vacancy ordering, modifying substantially the calculated

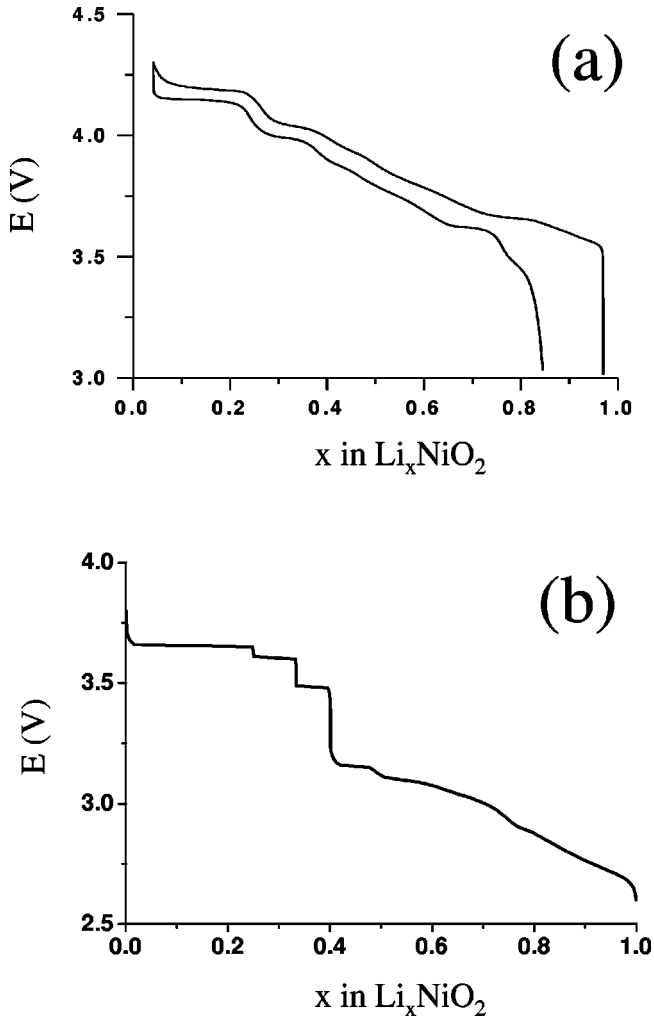


FIG. 8. Comparison between the (a) experimental and (b) calculated voltage-composition curves of a Li//LiNiO₂ cell. The experimental data are courtesy of Delmas *et al.* (Ref. 17) and shows both a charge and a discharge curve.

phase diagram. The disorder introduced by the Ni excess can also affect the phase transformations.

E. Voltage-composition curve

Monte Carlo simulations give the chemical potential as a function of concentration. The equilibrium potential of an electrochemical lithium cell depends on the chemical-potential difference for lithium in the anode and cathode materials:

$$\phi(x) = -[\mu_{\text{Li}}^{\text{cathode}}(x) - \mu_{\text{Li}}^{\text{anode}}(x)]/e, \quad (3)$$

where μ_{Li} is the lithium chemical potential in eV. If the anode potential is taken as the standard chemical potential for metallic lithium, the cell potential is simply given by the negative of the chemical potential for lithium in the cathode, which is directly obtainable from the Monte Carlo simulation.

Though the voltage-composition curve contains the same information as the phase diagram, it allows a better compari-

son with the experimental data. Figure 8 shows the experimental and the calculated voltage-composition curve of a Li//LiNiO₂ cell at room temperature (experimental data from Ref. 17). The calculated voltage is about 0.5 V below the experimental voltage, as is usual of voltages for lithium cells calculated within LDA and GGA.^{26,32,38,39} Nevertheless the intercalation reaction mechanism is reflected in the shape of the voltage-composition curve. In the two-phase domains the cell voltage remains constant whereas the single-phase areas are characterized by continuous changes in the cell voltage. These voltage changes are gradual in the solid solution ranges and abrupt in the regions where the lithium ions order. The shape of the calculated voltage-composition curve [Fig. 8(b)] is very similar to the experimental one [Fig. 8(a)], though some discrepancy exists in the $0 < x < 0.4$ region. In the calculated data two ordered phases appear at $x=0.25$ and $x=1/3$. This is in agreement with the electron-diffraction study in Li_{0.28}Ni_{1.02}O₂, which revealed the presence of ordered Li_{0.25}NiO₂ and Li_{0.33}NiO₂ structures.^{17,48} Contrary to this, in the experimental curve a unique voltage drop is observed around $x \approx 0.27$, instead of the two voltage steps at $x=1/4$ and $1/3$. We believe that the experimental conditions could hide the real equilibrium voltage drops resulting from the ordered phases Li_{0.25}NiO₂ and Li_{0.33}NiO₂. In fact, galvanostatic cycling of a Li//LiNiO₂ cell at a low rate ($C/100$) has shown these two voltage steps.³⁷

V. SUMMARY

We have performed a first-principles investigation of phase stability in Li_{*x*}NiO₂ for $0 < x < 1$. The most stable lithium-vacancy arrangements for Li_{1/4}NiO₂ and Li_{1/3}NiO₂ in the calculations agree with the experimental models based on electron-diffraction data. We, furthermore, predicted particular ordered configurations at compositions Li_{3/4}NiO₂ and Li_{1/2}NiO₂, where ordering has been postulated in the literature but no experimental characterization has been performed. In the region $0.5 < x < 0.75$ first-principles calculations are inconsistent with the model proposed previously to explain the ordering found in a sample of nominal composition Li_{0.63}Ni_{1.02}O₂.^{20,47} At Li_{2/5}NiO₂, where ordering has not previously been considered, we predict a very stable phase with rows of nearest-neighbor Li-Li dumbbells.

The Li-vacancy ordering differs considerably between LiCoO₂ and LiNiO₂. In Li_{*x*}CoO₂ two ordered states at $x=1/3$ and $1/2$ are predicted at room temperature. This situation contrasts with the calculated Li_{*x*}NiO₂ phase diagram where ordered states appear at $x=1/4$, $1/3$, $2/5$, $1/2$, and $3/4$ in the O3 host near room temperature. In both LiCoO₂ and LiNiO₂ we found strongly screened in-plane lithium-lithium interactions. However, unlike in Li_{*x*}CoO₂, the stability of ordered Li_{*x*}NiO₂ structures is also determined by long-range attractive interplane lithium-lithium interactions, related to the charge distribution and electronic structure of Ni. Therefore, the driving force for the distinct Li-Li interaction, and ultimately the different phase stability found in Li_{*x*}NiO₂ and Li_{*x*}CoO₂, is due to the electronic nature of the transition-metal cations.

ACKNOWLEDGMENTS

This work was supported by the Department of Energy under Grant No. DE-FG02-96ER 45571. Support from the Singapore-MIT Alliance is gratefully acknowledged. We express our sincere gratitude to C. Mariannetti for insightful

contributions on parts of the work presented here. We also thank Professor Delmas for helpful discussion on this work. G.C. acknowledges support from Umicore. This research was supported in part by the NSF cooperative agreement ACI-9619020 through computing resources provided by the National partnership for Advanced Computational Infrastructure at the San Diego Supercomputer Center.

- ¹B. Amundsen and J. Paulsen, *Adv. Mater.* **13**, 943 (2001).
- ²C. Delmas, J.P. Peres, A. Rougier, A. Demourges, F. Weill, A. Chadwick, M. Broussely, F. Pertont, Ph. Biensan, and P. Willmann, *J. Power Sources* **68**, 120 (1997).
- ³J.N. Reimers and J.R. Dahn, *J. Electrochem. Soc.* **139**, 2091 (1992).
- ⁴T. Ohzuku and A. Ueda, *J. Electrochem. Soc.* **141**, 2972 (1994).
- ⁵A. Van der Ven, M.K. Aydinol, G. Ceder, G. Kresse, and J. Hafner, *Phys. Rev. B* **58**, 2975 (1998).
- ⁶G. Ceder and A. Van der Ven, *Electrochim. Acta* **45**, 131 (1999).
- ⁷J.B. Goodenough, D.G. Wickham and W.J. Croft, *J. Phys. Chem. Solids* **5**, 107 (1958).
- ⁸A. Rougier, C. Delmas, and A.V. Chadwick, *Solid State Commun.* **94**, 123 (1995).
- ⁹M.G.S.R. Thomas, W.I.F. David, J.B. Goodenough, and P. Groves, *Mater. Res. Bull.* **20**, 1137 (1985).
- ¹⁰J.R. Dahn, U. von Sacken, and C.A. Michal, *Solid State Ionics* **44**, 87 (1990).
- ¹¹G. Dutta, A. Manthiram, J.B. Goodenough, and J.-C. Grenier, *J. Solid State Chem.* **96**, 123 (1992).
- ¹²R. Kanno, H. Kubo, Y. Kawamoto, T. Kamiyama, F. Izumi, Y. Takeda, and M. Takano, *J. Solid State Chem.* **110**, 216 (1994).
- ¹³T. Ohzuku, A. Ueda, and M. Nagayama, *J. Electrochem. Soc.* **140**, 1862 (1993).
- ¹⁴W. Li, J.N. Reimers, and J.R. Dahn, *Solid State Ionics* **67**, 123 (1993).
- ¹⁵H. Arai, S. Okada, H. Ohtsuka, M. Ichimura, and J. Yamaki, *Solid State Ionics* **80**, 261 (1995).
- ¹⁶A. Hirano, R. Kanno, Y. Kawamoto, Y. Takeda, K. Yamaura, M. Takano, K. Ohyama, M. Ohashi and Y. Yamaguchi, *Solid State Ionics* **78**, 123 (1995).
- ¹⁷C. Delmas, M. Menetrier, L. Croguennec, S. Levasseur, J.P. Peres, C. Pouillierie, G. Prado, L. Fournes, and F. Weill, *Int. J. Inorg. Mater.* **1**, 11 (1999).
- ¹⁸X.Q. Yang, X. Sun, and J. McBreen, *Electrochem. Commun.* **1**, 227 (1999).
- ¹⁹H. Arai, S. Okada, Y. Sakurai, and J. Yamaki, *Solid State Ionics* **95**, 275 (1997).
- ²⁰J.P. Peres, F. Weill, C. Delmas, *Solid State Ionics* **116**, 19 (1999).
- ²¹J. Morales, C. Perez-Vicente, and J.L. Tirado, *Mater. Res. Bull.* **25**, 623 (1990).
- ²²A. Rougier, P. Gravereau, and C. Delmas, *J. Electrochem. Soc.* **143**, 1169 (1996).
- ²³J.P. Peres, C. Delmas, A. Rougier, M. Broussely, F. Pertont, P. Biensan, and P. Willmann, *J. Phys. Chem. Solids* **57**, 1057 (1996).
- ²⁴A. Hirano, R. Kanno, Y. Kawamoto, K. Oikawa, T. Kamiyama, and F. Izumi, *Solid State Ionics* **86-88**, 791 (1996).
- ²⁵G. Ceder, Y.M. Chiang, D.R. Sadoway, M.K. Aydinol, Y.I. Jang, B. Huang, *Nature (London)* **392**, 694 (1998).
- ²⁶J.S. Braithwaite, C.R.A. Catlow, J.D. Gale, J.H. Harding, and P.E. Ngoepe, *J. Mater. Chem.* **10**, 239 (2000).
- ²⁷C. Wolverton and A. Zunger, *Phys. Rev. B* **57**, 2242 (1998).
- ²⁸A. Van der Ven and G. Ceder, *Electrochem. Solid-State Lett.* **3**, 301 (2000).
- ²⁹M.K. Aydinol, A.F. Kohan, and G. Ceder, *J. Power Sources* **68**, 664 (1997).
- ³⁰G. Kresse and J. Furthmuller, *Comput. Mater. Sci.* **6**, 15 (1996).
- ³¹G. Kresse and J. Furthmuller, *Phys. Rev. B* **54**, 11 169 (1996).
- ³²S.K. Mishra and G. Ceder, *Phys. Rev. B* **59**, 6120 (1999).
- ³³M.E. Arroyo y de Dompablo, C. Marianetti, A. Van der Ven, and G. Ceder, *Phys. Rev. B* **63**, 144107 (2000).
- ³⁴A. van de Walle and G. Ceder, *J. Phase Equilib.* (to be published).
- ³⁵G.G. Amatucci, J.M. Tarascon, and L.C. Klein, *J. Electrochem. Soc.* **143**, 1114 (1996).
- ³⁶A. Van der Ven, M.K. Aydinol, and G. Ceder, *J. Electrochem. Soc.* **145**, 2149 (1998).
- ³⁷L. Croguennec, C. Pouillierie, and C. Delmas, *J. Electrochem. Soc.* **147**, 1314 (2000).
- ³⁸M.K. Aydinol, A.F. Kohan, G. Ceder, K. Cho, and J. Joannopoulos, *Phys. Rev. B* **56**, 1354 (1997).
- ³⁹G. Ceder, M.K. Aydinol, and A.F. Kohan, *Comput. Mater. Sci.* **8**, 161 (1997).
- ⁴⁰F. Ducastelle, *Order and Phase Stability in Alloys* (North-Holland, Amsterdam, 1991).
- ⁴¹J.M. Sanchez, F. Ducastelle, and D. Gratias, *Physica A* **128**, 334 (1984).
- ⁴²K. Binder and D. W. Heermann, *Monte Carlo Simulation in Statistical Physics* (Springer-Verlag, Berlin, 1988).
- ⁴³M. Kaburagi and J. Kanamori, *Jpn. J. Appl. Phys., Suppl.* **2**, 145 (1974).
- ⁴⁴M. Kaburagi and J. Kanamori, *J. Phys. Soc. Jpn.* **44**, 718 (1978).
- ⁴⁵A. Ueda and T. Ohzuku, *J. Electrochem. Soc.* **141**, 2010 (1994).
- ⁴⁶I. Saadoune and C. Delmas, *J. Solid State Chem.* **136**, 8 (1998).
- ⁴⁷J.P. Peres, A. Demourges, and C. Delmas, *Solid State Ionics* **111**, 135 (1998).
- ⁴⁸J. P. Peres, Doctoral thesis, L'Universit e Bordeaux I, 1996.
- ⁴⁹V. Bianchi, S. Bach, C. Belhomme, J. Farcy, J. P. Pereira-Ramos, D. Caurant, N. Baffier, and P. Willmann, *Electrochim. Acta* **46**, 999 (2001).